#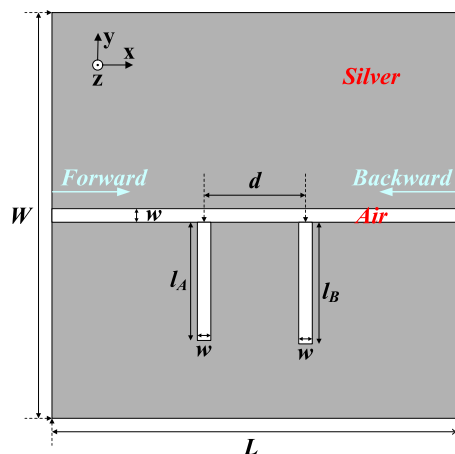 Unidirectional Reflectionless Propagation in Plasmonic Waveguide System Based on Phase Coupling Between Two Stub Resonators

Cong Zhang
Ruiping Bai
Xintong Gu
Xing Ri Jin
Ying Qiao Zhang
YoungPak Lee

Unidirectional Reflectionless Propagation in Plasmonic Waveguide System Based on Phase Coupling Between Two Stub Resonators

Cong Zhang,[1] **Ruiping Bai,**[1] **Xintong Gu,**[1] **Xing Ri Jin** 🄾**,**[1]
Ying Qiao Zhang,[1] **and YoungPak Lee**[2]

[1]Department of Physics, College of Science, Yanbian University, Jilin 133002, China
[2]Quantum Photonic Science Research Center and the Department of Physics, Hanyang University, Seoul 133-791, South Korea

Abstract: A scheme on unidirectional reflectionless propagation is theoretically investigated in a plasmonic waveguide system which consists of two metal–insulator–metal (MIM) stub resonators side coupled to an MIM plasmonic waveguide. By appropriately tuning the phase difference between two stub resonators, unidirectional reflectionless propagation at exceptional point, phase transition, and coherent perfect absorber are realized. Moreover, in both directions, reflectivity for one side is close to 0 and for the other side approximates to 0.8.

Index Terms: Plasmonic waveguide, phase coupling, unidirectional reflectionlessness, exceptional point

1. Introduction

Ever since Bender and colleagues proposed that real eigenvalue spectra could be obtained in a wide class of complex non-Hermitian Hamiltonians with parity-time (PT) symmetry [1], [2], more and more optical systems have been explored due to the isomorphism between Schrödinger equation and optical wave equation. To exhibit the properties of non-Hermitian Hamiltonians, a range of associated extraordinary phenomena have been studied, including unidirectional transmission [3], [4], induced optical transparency [5], [6], coherent perfect absorber [7], [8], absorber-amplifier [9], [10], loss-induced super scattering and gain-induced absorption [11], polarization of terahertz metasurfaces [12], lasers [13]–[16], non-reciprocal light propagation [17]–[22], unidirectional reflectionlessness [23]–[31], and so on. Among these, unidirectional reflectionlessness has aroused considerable interests in optical domain due to that such relevant structures likely substitute optical filter, sensor and diode [23]–[31]. By modulating the real and imaginary parts of refractive index or

the ratio of gain and loss, unidirectional reflectionless phenomenon was obtained in some PT optical structures including periodic grating [23], zero index metamaterial [24], and metasurfaces [25].

Besides, unidirectional reflectionless phenomenon has also been obtained in non-Hermitian Hamiltonians system without meeting the balanced gain and loss [26]–[31]. Firstly, unidirectional reflectionlessness was demonstrated experimentally in passive(no gain) optical waveguide by Feng *et al.* in 2013 [26]. Whereafter, they once again achieved unidirectional reflectionless phenomenon in a large-size optical multilayer structure with absorbing and non-absorbing dielectrics at visible frequencies [27]. In the recent years, increasing attentions have been attracted to plasmonic waveguide structures [30]–[40] for that surface plasmon polaritons (SPPs) can control light at nanoscale beyond the diffractive limit and their capabilities to easily integrated into photonic circuits and to achieve ultracompact optical devices as well. As the further research on the properties of non-Hermitian Hamiltonians, Huang *et al.* [30] attained unidirectional reflectionless propagation by tuning geometric parameters of the structures in non-PT symmetric plasmonic waveguide-cavity system in 2015. In their structure, to achieve the greater reflectivity difference between the forward and backward directions, one of the identical-frequency resonators is required to be lower loss, i.e., the smaller width for this resonator is required to meet the higher quality factor. Moreover, even if their resonators are low loss, a large reflectivity difference is difficult to realize. Subsequently, Huang *et al.* [31] reconstructed a structure with unbalanced gain and loss, in which two stub resonators were filled with silicon dioxide doped with CdSe (loss) and InGaAsP (gain), respectively, for the purpose of increasing the reflectivity difference between the forward and backward directions close to unity.

In this work, a plasmonic waveguide structure consists of two metal-insulator-metal (MIM) stub resonators side coupled to a MIM plasmonic waveguide is designed. The two stub resonators have the almost identical quality factor at different frequencies. Based on phase coupling of the two stub resonators, unidirectional reflectionless phenomenon is realized at EP. By adjusting phase difference between two stub resonators, phase transitions from Hermitian to non-Hermitian and from nonideal PT symmetry to symmetry breaking, as well as coherent perfect absorber (CPA) are obtained. The dimension of our structure is smaller than SPP propagation length [32], so the loss is largely lowered. Noteworthily, our plasmonic waveguide structure dopes with no gain or loss media and doesn't demand the smaller width for the stub resonator, it is more easier to fabricate through experiment.

2. Results and Discussion

The schematic diagram of the proposed plasmonic structure with two stub resonators is illustrated in Fig. 1. Distance d between two stub resonators is variable and length l_A (l_B) of the stub resonator is 625 nm (660 nm). Parameter $w = 50$ nm represents the widths of plasmonic waveguide and stub resonators. Both the length L and width W of the structure are 2000 nm in simulation. The dielectric of the two stub resonators and waveguide is air and the metal is silver. The relative permittivity of silver is described by Drude model with the plasmon frequency ω_p of 1.366×10^{16} rad/s and the collision frequency ω_c of 3.07×10^{13} Hz [41], [42]. The numerical simulation is carried out by employing a finite-integration package (CST Microwave Studio). And the boundary conditions of system are magnetic ($H_t = 0$) in X_{min}, X_{max}, Z_{min}, and Z_{max}, and electric ($E_t = 0$) at Y_{min} and Y_{max}.

Fig. 2(a) and (b) depicts the reflection spectra for both forward and backward directions by using numerical simulation and analytical calculation (scattering matrix theory), respectively. The magenta short dash-dot line, dark cyan dashed line, blue short dashed line, red short dotted line and gray solid line exhibit the reflection spectra (numerical simulation) for distance $d = 423$, 440, 450, 460 and 478 nm, respectively. From Fig. 2(a), the reflection dip shifts toward low frequencies (red-shift) and reflectivity decreases with the increasing distance d for the case of the forward direction. In Fig. 2(b), the reflection dip shifts toward low frequencies and reflectivity increases with the increasing distance d for the backward direction. Unidirectional reflectionless phenomena appear at frequencies 243.96 THz and 251.44 THz, respectively, based on the phase coupling of the two resonators. For example, when $d = 478$ nm, reflectivity at 243.96 THz in forward direction is
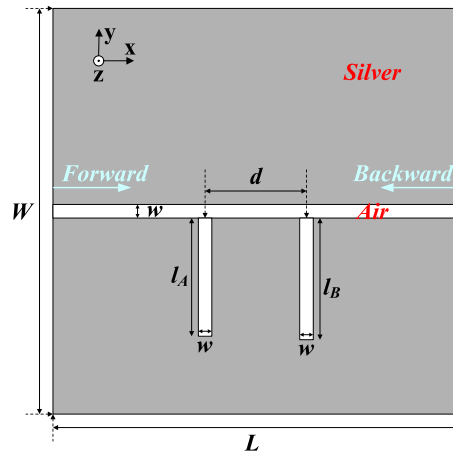
Fig. 1. Schematic diagram of a pair of stub resonators side coupled to a MIM waveguide. The geometric parameters of the structure are l_A = 625 nm, l_B = 660 nm, w = 50 nm, $L = W$ = 2000 nm, while d is variable.
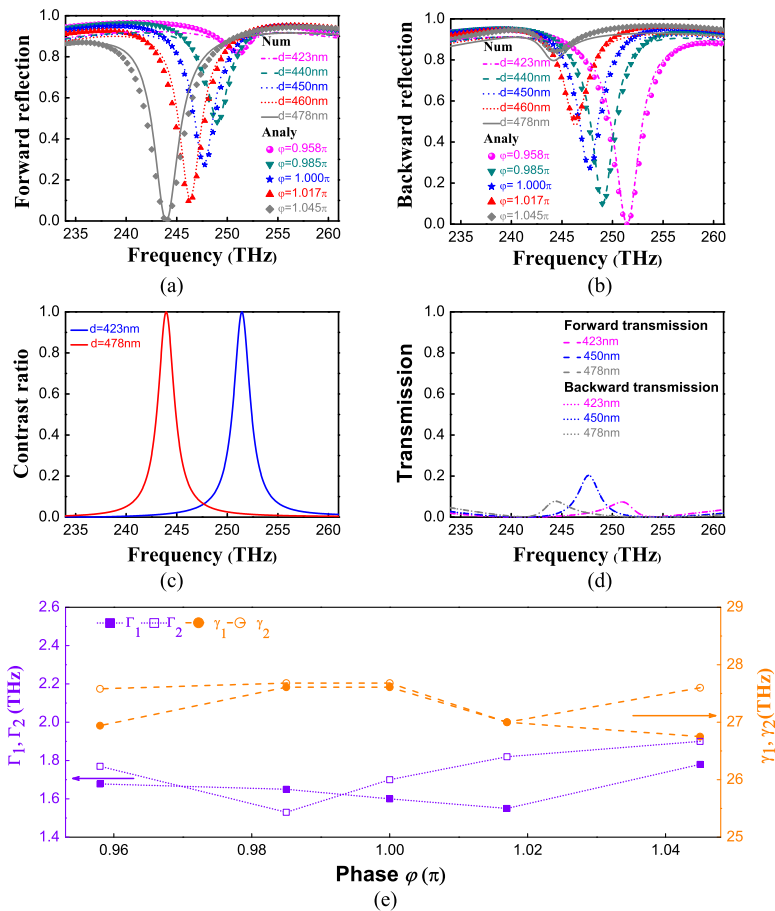
Fig. 2. Reflection spectra of forward (a) and backward (b) directions with different distance d and phase difference φ based on numerical simulation (Num) and analytical calculation (Analy). (c) The contrast ratios between the forward reflection R_f and backward reflection R_b for the distance d = 423 nm and 478 nm versus frequency ω. (d) Forward and backward transmission spectra with d = 423 nm, d = 450 nm, and d = 478 nm. (e) The relevant parameters $\gamma_{1(2)}$ and $\Gamma_{1(2)}$ versus phase difference φ.

Fig. 3. The z-component distributions of magnetic field of the SPPs at frequencies 251.44 THz and 243.96 THz for the forward and backward directions. (a) and (b) correspond to the forward and backward propagating SPPs for the case of $d = 423$ nm at 251.44 THz, respectively. (c) and (d) correspond to that of $d = 478$ nm at 243.96 THz.

close to 0, while it is bigger than 0.8 in backward direction. It is clear that great reflectivity difference between two directions is realized in our low-loss plasmonic waveguide s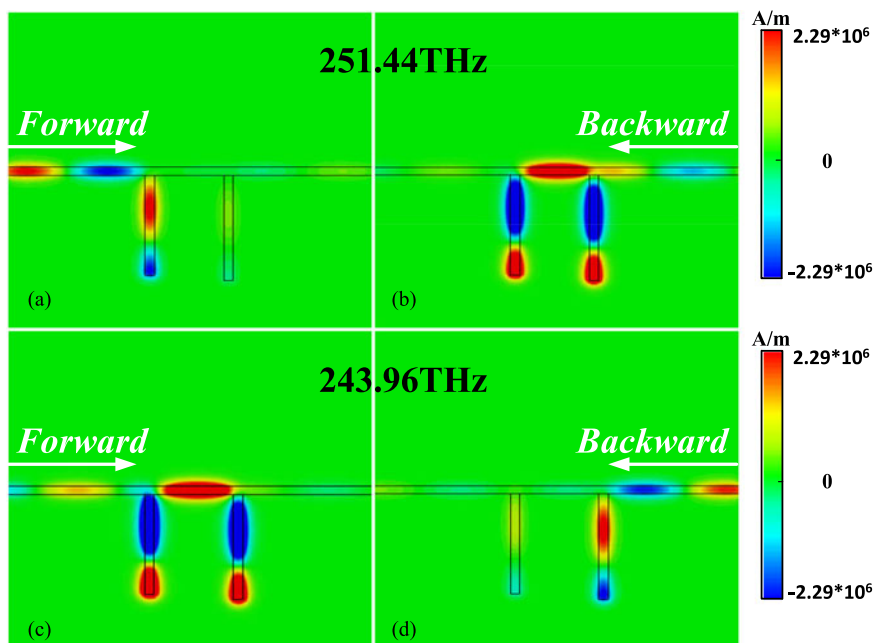tructure. Moreover, when distance $d = 450$ nm, reflection spectra for both forward and backward directions are the same. Additionally, the contrast ratios between the forward reflection R_f and backward reflection R_b defined as $|(R_f - R_b)/(R_f + R_b)|$ are plotted in Fig. 2(c) with $d = 423$ nm (blue solid line) and 478 nm (red solid line), respectively. The contrast ratios of near 1 emerge at frequencies 251.44 THz and 243.96 THz, respectively. Fig. 2(d) shows the transmission spectra of forward and backward directions in numerical simulation. The magenta, blue, and gray dash (short dotted) lines correspond to forward (backward) transmission spectra with $d = 423$ nm, 450 nm, and 478 nm, respectively. We notice that the forward and backward transmission curves are superposed, and low transmissivities occur at 251.44 THz and 243.96 THz for $d = 423$ nm and 478 nm, respectively.

In order to intuitively exhibit the unidirectional reflectionless phenomena, we display the z-component distributions of magnetic field of the SPPs in Fig. 3 by employing numerical simulation. Fig. 3(a) and (b) are the z-component distributions of magnetic field in the forward and backward directions with $d = 423$ nm at 251.44 THz, respectively, and Fig. 3(c) and (d) correspond to the case of $d = 478$ nm at 243.96 THz, respectively. From Fig. 3(a), (d), the distribution of magnetic field of right (left) stub resonator is almost minimum while the left (right) is maximum, which demonstrates that the phase difference between two resonators approximates to $3\pi/2$. And the distributions of magnetic field for two resonators are maximum according to Fig. 3(b) and (c), which indicates that the phase difference between two resonators is 2π. Hence, the high and low reflections appear when phase difference $\sim 3\pi/2$ (Fig. 3(a) and (d)) and $\sim 2\pi$ (Fig. 3(b) and (c)), respectively, based on the Fabry-Pérot (FP) resonance coupling between the two stub resonators. As expected, from Fig. 3(b) and (c), weak reflections occur in backward and forward directions at frequencies 251.44 THz and 243.96 THz, respectively, while strong reflections occur in forward and backward directions at frequencies 251.44 THz and 243.96 THz (Fig. 3(a) and (d)), respectively. Therefore, unidirectional reflectionless phenomenon appears at EP for $d = 423$ nm (478 nm) at 251.44 THz (243.96 THz) based on FP resonance coupling.

In order to further elucidate our scheme, we employ scattering matrix to analyze the properties of the plasmonic waveguide system. In a general case, corresponding to the plasmonic waveguide structure in Fig. 1, the scattering properties for a surface plasmon of frequency ω can be expressed by the transfer matrix T_{all} [41]

$$T_{all} = T_s^1 \times T_p \times T_s^2 = \begin{pmatrix} T_{11} & T_{12} \\ T_{21} & T_{22} \end{pmatrix}, \tag{1}$$

with

$$T_s^{1(2)} = \begin{pmatrix} 1 - \dfrac{i\gamma_{1(2)}}{\omega - \omega_{1(2)} + i\Gamma_{1(2)}} & \dfrac{-i\gamma_{1(2)}}{\omega - \omega_{1(2)} + i\Gamma_{1(2)}} \\ \dfrac{i\gamma_{1(2)}}{\omega - \omega_{1(2)} + i\Gamma_{1(2)}} & 1 + \dfrac{i\gamma_{1(2)}}{\omega - \omega_{1(2)} + i\Gamma_{1(2)}} \end{pmatrix}, \tag{2}$$

and

$$T_p = \begin{pmatrix} \exp(i\varphi) & 0 \\ 0 & \exp(-i\varphi) \end{pmatrix}, \tag{3}$$

where $T_s^{1(2)}$ and T_p are transfer matrices for the scattering properties of the left (right) resonator and for the phase shift of the surface plasmon propagating from the left stub resonator to the right one. $\omega_{1(2)}$, $\gamma_{1(2)}$ and $\Gamma_{1(2)}$ are the resonance frequency, the width of the resonance and the loss of the left (right) stub resonator, respectively. φ is the accumulated phase shift for SPPs propagating between two stub resonators. So, according to the transfer matrix T_{all}, the corresponding reflection and transmission coefficients can be given as

$$r_f = \frac{-T_{21}}{T_{22}}, \ \ r_b = \frac{T_{12}}{T_{22}} \ \text{and} \ \mathrm{t} = \mathrm{t_f} = \mathrm{t_b} = \frac{1}{T_{22}}, \tag{4}$$

where r_f and r_b are the complex reflection coefficients for SPPs propagating from the left (forward) and right (backward) directions, respectively, while t_f and t_b are the complex transmission coefficients for SPPs propagating from the left (forward) and right (backward) directions, respectively. In our plasmonic waveguide system, $|r_f|^2$ and $|r_b|^2$ are not identical, while $|t_f|^2$ is equal to $|t_b|^2$.

For the purpose of proving the validity of the numerical simulation, we exhibit the reflection spectra (analytical c alculation) as the function of frequency ω with different phase differences φ based on (4) in Fig. 2. In Fig. 2(a) and (b), magenta solid-sphere, dark cyan down-solid-triangle, blue solid-star, red up-solid-triangle and gray solid-diamond lines clearly show the reflection spectra for phase differences $\varphi = 0.958\pi$, 0.985π, π, 1.017π and 1.045π, respectively. From Fig. 2(a) and (b), the reflection dip has a red-shift and the reflectivity decreases (increases) with the increasing phase φ for the forward (backward) direction, which is in good agreement with the result of the numerical simulation. Obviously, unidirectional reflectionless phenomena appear at frequencies 243.96 THz and 251.44 THz, respectively. And the reflection spectra for both for ward and backward directions are the same when phase $\varphi = \pi$. The involved parameters $\gamma_{1(2)}$ and $\Gamma_{1(2)}$ are shown in Fig. 2(e), from which parameters $\gamma_{1(2)}$ and $\Gamma_{1(2)}$ don't change evidently with the variation of phase difference φ.

Following, in order to prove the uniformity between numerical simulation and analytical calculation further, we plot the reflection spectra versus frequency ω and phase φ for the forward and backward propagating SPPs by utilizing (4) in Fig. 4(c) and (d), respectively. We notice that unidirectional reflectionless phenomena occur in two frequency ranges of 241 THz~247 THz and 249 THz~255 THz (corresponding to φ of $1.048\pi \sim 1.013\pi$ and $0.972\pi \sim 0.924\pi$) for the forward and backward directions, respectively. In other word, the low reflection region (blue region) for the forward direction (Fig. 4(c)) corresponds to the high reflection region for the backward direction (Fig. 4(d)), and vice versa. From Fig. 4(a), (b) and (c), (d), reflection peaks of different phases φ match well with that of different distances d. Therefore, the reflections obtained by analytical calculation are in good agreements with that by numerical simulation.
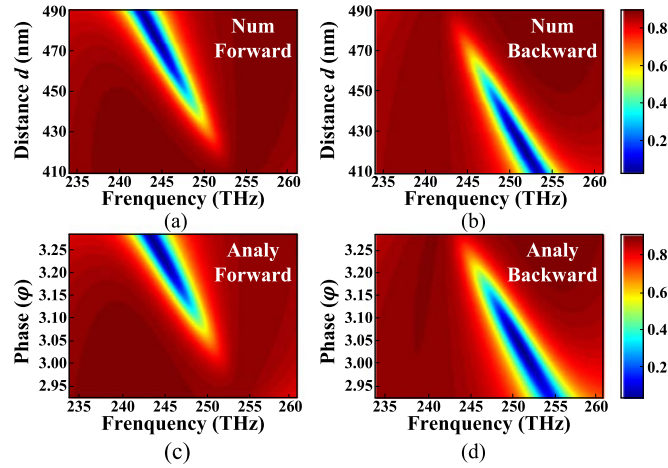
Fig. 4. Dependence of reflectivity on distance d and frequency ω of the propagating SPPs for the forward (a) and backward (b) directions based on numerical simulation. (c) and (d) are the dependence of reflectivity on phase φ and frequency ω for the forward and backward directions based on analytical calculation, respectively. The corresponding parameters of analytical calculation γ_1, γ_2, Γ_1 and Γ_2 are 26.94 THz, 27.58 THz, 1.678 THz and 1.77 THz, respectively.

Furthermore, the phase shift $\varphi_{1(2)}$ for the left (right) resonator in the forward and backward directions can be obtained by (2) as [32], [41]

$$\varphi_{1(2)} = \arctan\left[\frac{\mathrm{Im}(T_{s21}^{1(2)}/T_{s22}^{1(2)})}{\mathrm{Re}\left(T_{s21}^{1(2)}/T_{s22}^{1(2)}\right)}\right] = \frac{\omega - \omega_{1(2)}}{\gamma_{1(2)} + \Gamma_{1(2)}}. \tag{5}$$

In our structure, phase difference φ_{all} between two resonators consists of three parts: the respective phase shifts of two resonators and the phase shift for SPPs propagation between two resonators. Therefore, φ_{all} in the forward and backward directions are $\varphi_1 - \varphi_2 + 2\varphi$ and $\varphi_2 - \varphi_1 + 2\varphi$, respectively. Based on Eq. (5) and some relevant parameters, both φ_{all} approaching 2π at 243.96 THz and 251.44 THz can be obtained in forward and backward directions, which results in that the reflection approximating to 0. Considering that z-component distributions of magnetic field for two stub resonators are in the same directions (Fig. 3(b) and (c)), phase difference between the two resonators are about 2π at 243.96 THz and 251.44 THz in the forward and backward directions, respectively.

Then we discuss the properties of the eigenvalues of scattering matrix S. Utilizing (4), the scattering matrix S of non-Hermitian can be written as [26]

$$S = \begin{pmatrix} t & r_b \\ r_f & t \end{pmatrix}, \tag{6}$$

and the corresponding eigenvalues can be expressed as

$$s_{\pm} = t \pm \sqrt{r_f r_b}. \tag{7}$$

When $\sqrt{r_f r_b}$ is zero, two eigenvalues coalesce and EP appears. This is to say, when $r_f = 0$, $r_b \neq 0$ ($r_b = 0$, $r_f \neq 0$), unidirectional reflectionlessness appears in the forward (backward) direction. Here, for t is real or complex, the non-Hermitian system is called an ideal PT or nonideal PT system [8].

The real and imaginary parts of the eigenvalues $s_{\pm}$ of scattering matrix S as the function of frequency ω for the incident SPPs are depicted in Fig. 5, respectively, for $\varphi = 0.958\pi$, π and 1.045π. As expected, EP for $\varphi = 0.958\pi$ (Fig. 5(a) and (b)) and $\varphi = 1.045\pi$ (Fig. 5(e) and (f)) occurs at frequencies 251.44 THz and 243.96 THz, respectively. We can clearly see that two real parts coalesce into a point (see Fig. 5(a) and (e)) and two imaginary parts cross at frequencies 251.44 THz and 243.96 THz (see Fig. 5(b) and (f), which means that the same complex eigenvalue
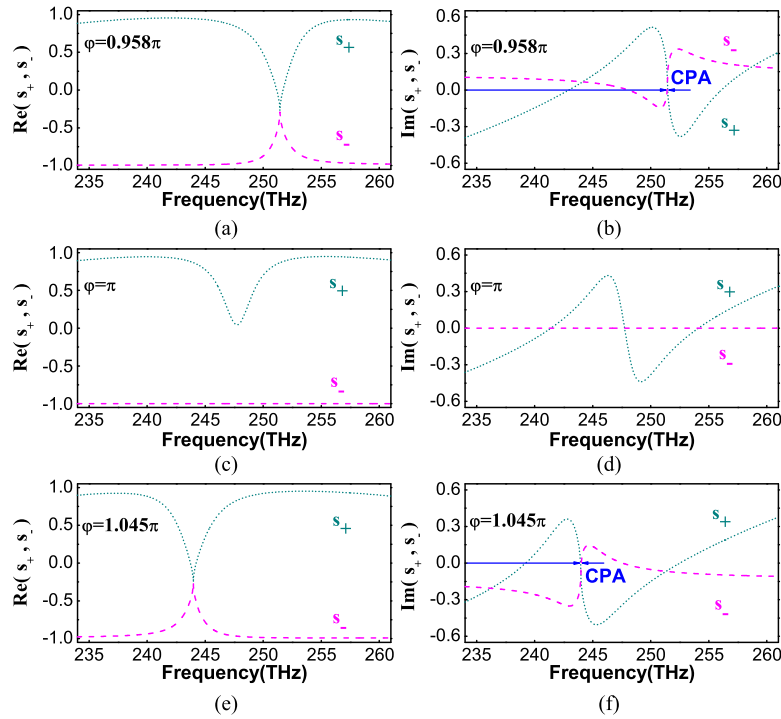
Fig. 5. The real (a), (c), (e) and imaginary (b), (d), (f) parts of the eigenvalues $s_{\pm}$ of scattering matrix S as the function of frequency ω for $\varphi = 0.958\pi$((a), (b)), π((c), (d)) and 1.045π((e), (f)), respectively. s_+ and s_- are represented by dark cyan short dotted line and magenta dashed line, respectively. Parameters γ_1, γ_2, Γ_1 and Γ_2 are the same as that in Fig. 2(e).

$s_+ = s_-$ occur. In this case, t is complex and $\sqrt{r_f r_b}$ is zero. Hence, by appropriately tuning the phase difference for SPPs propagation between two resonators, unidirectional reflectionlessness can be obtained at EP. The phase transition from nonideal PT symmetry to symmetry breaking appears at EP. In addition, in the case of the identical reflections for the forward and backward directions, two real parts of $s_{\pm}$ at 247.7 THz do not coalesce with each other (see Fig. 5(c)), while two imaginary parts of $s_{\pm}$ cross in a point at 247.7 THz and the imaginary part of s_- always equal to zero (see Fig. 5(d)). In this case, our plasmonic waveguide system is Hermitian. In other words, the phase transition from Hermitian to non-Hermitian at 247.7 THz appear for $\varphi = \pi$.

According to Eq. (7), for the complex t and $\sqrt{r_f r_b}$, some appropriate parameters can make one of the eigenvalues $s_{\pm}$ real while the other complex, which corresponding to the phenomenon of coherent perfect absorption (CPA) [8]. From Fig. 5(b), both imaginary parts of the eigenvalues $s_{\pm}$ are equal to zero at two points 251.4 THz and 251.5 THz (marked by two blue arrows), quite close to EP (251.44 THz), where CPAs appear. For the backward propagating SPPs, CPAs emerge, respectively, at 251.4 THz and 251.5 THz, the vicinity of EP, where the corresponding reflection approach 0 (see Fig. 2(b)) and the transmission close to 0. So, the absorption of about 0.92 can be obtained based on the formula $A = 1 - |t|^2 - |r_b|^2$. Moreover, both the quality factors related to the spectra of CPAs at frequencies 251.4 THz and 251.5 THz are about 68. The quality factor is defined as $f/\Delta f$, where f and Δf are resonant frequency and full width half maximum, respectively. Similarly, CPAs (marked by two blue arrows) for the forward direction appear, respectively, at frequencies 243.9 THz and 244 THz with $\varphi = 1.045\pi$ (see Fig. 5(f)). In this case, the absorptions of about 0.92 can be obtained with quality factors of about 61 at frequencies 243.9 THz and 244 THz, respectively, by formula $A = 1 - |t|^2 - |r_f|^2$. These show that our plasmonic waveguide system is PT symmetry breaking in CPA points. That is to say, the phase transition from nonideal-PT symmetry to symmetry breaking system appears in CPA points.

3. Conclusions

We demonstrate low-loss unidirectional reflectionless phenomenon at EP based on phase coupling between two stub resonators in a plasmonic waveguide structure. The reflectivity of one side approximates 0, while the other side is about 0.8 for the forward (backward) direction. More interestingly, by appropriately adjusting the phase coupling to between two stub resonators, phase transitions from Hermitian to non-Hermitian and nonideal PT symmetry to symmetry breaking, and two CPAs in the vicinity of EP are clearly observed, respectively. The absorptions of CPAs are all about 0.92 with quality factors over 60. Moreover, great reflectivity difference between two directions is realized in the low-loss structure, and there is no need to dope with any gain or loss and no requirements for the smaller width of the two stub resonators, which make our plasmonic waveguide structure easier to fabricate through experiments. We believe that our plasmononic waveguide structure can be easily to integrate into photonic circuits and achieve ultracompact optical devices to serve as the promising candidate of the filter, sensor, plasmonic diode-like device and so on.

References

[1] C. M. Bender and S. Boettcher, "Real spectra in non-Hermitian Hamiltonians having PT symmetry," *Phys. Rev. Lett.*, vol. 80, no. 24, pp. 5243–5246, Jun. 1998.

[2] C. M. Bender, "Making sense of non-Hermitian Hamiltonians," *Rep. Prog. Phys.*, vol. 70, no. 6, pp. 947–1018, May 2007.

[3] S. L. Zhang, Z. D. Yong, Y. G. Zhang, and S. L. He, "Parity-time symmetry breaking in coupled nanobeam cavities," *Sci. Rep.*, vol. 6, Apr. 2016, Art. no. 24487.

[4] Y. L. Xu, L. Feng, M. H. Lu, and Y. F. Chen, "Unidirectional transmission based on a passive PT symmetric grating with a nonlinear silicon distributed Bragg reflector cavity," *IEEE Photon. J.*, vol. 6, no. 1, Feb. 2014, Art. no. 0600507.

[5] A. Guo and G. J. Salamo, "Observation of PT-symmetry breaking in complex optical potentials," *Phys. Rev. Lett.*, vol. 103, no. 9, Aug. 2009, Art. no. 093902.

[6] H. Jing *et al.*, "Optomechanically-induced transparency in parity-time-symmetric microresonators," *Sci. Rep.*, vol. 5, Jun. 2015, Art. no. 09663.

[7] M. Kang, F. Liu, and J. Li, "Effective spontaneous PT-symmetry breaking in hybridized metamaterials," *Phys. Rev. A.*, vol. 87, no. 5, May 2013, Art. no. 053824.

[8] Y. Sun, W. Tan, H. Q. Li, J. Li, and H. Chen, "Experimental demonstration of a coherent perfect absorber with PT phase transition," *Phys. Rev. Lett.*, vol. 112, no. 14, Apr. 2014, Art. no. 143903.

[9] B. Baum, H. Alaeian, and J. A. Dionne, "A parity-time symmetric coherent plasmonic absorber-amplifier," *J. Appl. Phys.*, vol. 117, Jan. 2015, Art. no. 063106.

[10] C. Y. Huang, R. Zhang, J. L. Han, J. Zheng, and J. Q. Xu, "Type-II perfect absorption and amplification modes with controllable bandwidth in combined PT-symmetric and conventional Bragg-grating structures," *Phys. Rev. A.*, vol. 89, no. 2, Feb. 2014, Art. no. 023842.

[11] S. M. Feng, "Loss-induced super scattering and gain-induced absorption," *Opt. Exp.*, vol. 24, no. 2, pp. 1291–1304, Jan. 2016.

[12] M. Lawrence *et al.*, "Manifestation of PT symmetry breaking in polarization space with terahertz metasurfaces," *Phys. Rev. Lett.*, vol. 113, no. 9, Aug. 2014, Art. no. 093901.

[13] M. A. Miri, P. LiKamWa, and D. N. Christodoulides, "Large area single-mode parity-time-symmetric laser amplifiers," *Opt. Lett.*, vol. 37, no. 5, pp. 764–766, Mar. 2012.

[14] L. Feng, Z. J. Wong, R. M. Ma, Y. Wang, and X. Zhang, "Single-mode laser by parity-time symmetry breaking," *Science*, vol. 346, no. 6212, pp. 972–975, Nov. 2014.

[15] H. Hodaei, M. A. Miri, M. Heinrich, D. N. Christodoulides, and M. Khajavikhan, "Parity-time-symmetric microring lasers," *Science*, vol. 346, no. 6212, pp. 975–978, Nov. 2014.

[16] Q. H. Song *et al.*, "The combination of directional outputs and single-mode operation in circular microdisk with broken PT symmetry," *Opt. Exp.*, vol. 23, no. 19, pp. 24257–24264, Sep. 2015.

[17] C. E. Rüter, K. G. Makris, R. EI-Ganainy, D. N. Christodoulides, M. Segev, and D. Kip, "Observarion of parity-time symmetry in optics," *Nature Phys.*, vol. 6, pp. 192–195, Jan. 2010.

[18] L. Feng *et al.*, "Nonreciprocal light propagation in a silicon photonic circuit," *Science*, vol. 333, no. 6043, pp. 729–732, Aug. 2011.

[19] H. Alaeian and J. A. Dionne, "Parity-time-symmetric plasmonic metamaterials," *Phys. Rev. A.*, vol. 89, no. 3, Mar. 2014, Art. no. 033829.

[20] L. Chang *et al.*, "Parity-time symmetry and variable optical isolation in active-passive-coupled microresonators," *Nature Photon.*, vol. 8, pp. 524–529, Jun. 2014.

[21] B. Peng *et al.*, "Parity-time-symmetric whispering-gallery microcavities," *Nature Phys.*, vol. 10, pp. 394–398, Apr. 2014.

[22] M. Turduev *et al.*, "Two-dimensional complex parity-time-symmetric photonic structures," *Phys. Rev. A.*, vol. 91, no. 2, Feb. 2015, Art. no. 023825.

[23] Z. Lin, H. Ramezani, T. Eichelkraut, T. Kottos, H. Cao, and D. N. Christodoulides, "Unidirectinal invisibility induced by PT-symmetric periodic structures," *Phys. Rev. Lett.*, vol. 106, no. 21, May 2011, Art. no. 213901.

[24] Y. Y. Fu, Y. D. Xu, and H. Y. Chen, "Zero index metamaterials with PT symmetry in a waveguide system," *Opt. Exp.*, vol. 24, no. 2, pp. 1648–1657, Jan. 2016.

[25] D. L. Sounas, R. Fleury, and A. Alù, "Unidirectional cloaking based on metasurfaces with balanced loss and gain," *Phys. Rev. A.*, vol. 4, no. 1, Jul. 2015, Art. no. 014005.

[26] L. Feng *et al.*, "Experimental demonstration of a unidirectional reflectionless parity-time metamaterial at optical frequencies," *Nature Mater.*, vol. 12, pp. 108–113, Feb. 2013.

[27] L. Feng *et al.*, "Demonstration of a large-scale optical exceptional point structure," *Opt. Exp.*, vol. 22, no. 2, pp. 1760–1767, Jun. 2014.

[28] E. C. Yang, Y. H. Lu, Y. Wang, Y. M. Dai, and P. Wang, "nidirectional reflectionless phenomenon in periodic ternary layered material," *Opt. Exp.*, vol. 24, no. 13, pp. 14311–14321, Jun. 2016.

[29] Y. Shen, X. H. Deng, and L. Chen, "Unidirectional invisibility in a two-layer non-PT-symmetric slab," *Opt. Exp.*, vol. 22, no. 16, pp. 19440–19447, Aug. 2014.

[30] Y. Huang, G. Veronis, and C. J. Min, "Unidirectional reflectionless propagation in plasmonic waveguide-cavity systems at exceptional points," *Opt. Exp.*, vol. 23, no. 23, pp. 29882–29895, Nov. 2015.

[31] Y. Huang, C. J. Min, and G. Veronis, "Broadband near total light absorption in non-PT-symmetric waveguide-cavity systems," *Opt. Exp.*, vol. 24, no. 19, pp. 22219–22231, Sep. 2016.

[32] J. J. Chen, C. Wang, R. Zhang, and J. H. Xiao, "Multiple plasmon-induced transparencies in coupled-resonator systems," *Opt. Lett.* vol. 37, no. 24, pp. 5133–5135, Dec. 2012.

[33] H. Lu, X. M. Liu, D. Mao, and G. X. Wang, "Plasmonic nanosensor based on Fano resonance in waveguide-coupled resonators," *Opt. Lett.*, vol. 37, no. 18, pp. 3780–3782, Sep. 2012.

[34] H. Lu, X. M. Liu, D. Mao, Y. K. Gong, and G. X. Wang, "Induced transparency in nanoscale plasmonic resonator systems," *Opt. Lett.*, vol. 36, no. 16, pp. 3233–3235, Aug. 2011.

[35] X. J. Piao, S. Yu, and N. Park, "Control of Fano asymmetry in plasmon induced transparency and its application to plasmonic waveguide modulator," *Opt. Exp.*, vol. 20, no. 17, pp. 18994–18999, Aug. 2012.

[36] Y. Huang, C. J. Min, and G. Veronis, "Subwavelengh slow-light waveguides based on a plasmonic analogue of electromagnetically induced transparency," *Appl. Phys. Lett.*, vol. 99, no. 14, Oct. 2011, Art. no. 143117.

[37] Z. H. Han and S. I. Bozhevolnyi, "Plasmon-induced transparency with detuned ultracompact Fabry-Perot resonators in integrated plasmonic devices," *Opt. Exp.*, vol. 19, no. 4, pp. 3251–3257, Feb. 2011.

[38] D. F. Pile *et al.*, "Two-dimensionally localized modes of a nanoscale gap plasmon waveguide," *Appl. Phys. Lett.*, vol. 87, no. 26, Dec. 2005, Art. no. 261114.

[39] Y. Matsuzaki, T. Okamoto, M. Haraguchi, M. Fukui, and M. Nakagaki, "Characteristics of gap plasmon waveguide with stub structures," *Opt. Exp.*, vol. 16, no. 21, pp. 16314–16325, Sep. 2008.

[40] W. Shin, W. Cai, P. B. Catrysse, G. Veronis, M. L. Brongersma, and S. H. Fan, "Broadband sharp 90-degree bends and tsplitters in plasmonic coaxial waveguides," *Nano Lett.*, vol. 13, no. 10, pp. 4753–4758, Aug. 2013.

[41] X. R. Jin, Y. Q. Zhang, S. Zhang, Y. P. Lee, and J. Y. Rhee, "Polarization-independent electromagnetically induced transparency-like effects in stacked metamaterials based on Fabry-Pérot resonance," *J. Opt.*, vol. 15, no. 12, Nov. 2013, Art. no. 125104.

[42] M. A. Ordal *et al.*, "Optical properties of the metals Al, Co, Cu, Au, Fe, Pb, Ni, Pd, Pt, Ag, Ti, and W in the infrared and far infrared," *Appl. Opt.*, vol. 22, no. 7, pp. 1099–1120, Apr. 1983.